Gas-Phase Structure, Rotational Barrier, and Vibrational Properties of Methyl Methanethiosulfonate, $CH_3SO_2SCH_3$: An Experimental and Computational Study

María E. Tuttolomondo,[†] Amparo Navarro,[‡] Tomás Peña Ruiz,[‡] Eduardo L. Varetti,[§,#] Stuart A. Hayes,[||] Derek A. Wann,[||] Heather E. Robertson,[||] David W. H. Rankin,[||] and Aida Ben Altabef*[,†,#]

Instituto de Química Física, Facultad de Bioquímica, Química y Farmacia, Universidad Nacional de Tucumán, San Lorenzo 456, 4000 Tucumán, R. Argentina, Departamento de Química Física y Analítica, Universidad de Jaén, Campus Las Lagunillas, 23071 Jaén, España, Centro de Química Inorgánica (CEQUINOR, CONICET-UNLP), Departamento de Química, Facultad de Ciencias Exactas, Universidad Nacional de La Plata, C. Correo 962, 1900 La Plata, R. Argentina, and School of Chemistry, University of Edinburgh, West Mains Road, Edinburgh, United Kingdom EH9 3JJ

Received: May 11, 2007; In Final Form: July 5, 2007

The molecular structure of methyl methanethiosulfonate, $CH_3SO_2SCH_3$, has been determined in the gas phase from electron-diffraction data supplemented by ab initio (HF, MP2) and density functional theory (DFT) calculations using 6-31G(d), 6-311++G(d,p), and 6-311G(3df,3pd) basis sets. Both experimental and theoretical data indicate that although both anti and gauche conformers are possible by rotating about the S−S bond, the preferred conformation is gauche. The barrier to internal rotation in the CSSC skeleton has been calculated using the RHF/6-31G(d), MP2/6-31G(d), and B3LYP/6-31G(d) methods as well as MP2 with a 6-31G(3df) basis set on sulfur and 6-31G(d) on C, H, and O. A 6-fold decomposition of the rotational barrier has been performed in terms of a Fourier-type expansion, enabling us to analyze the nature of the potential function, showing that the coefficients V_1 and V_2 are the dominant terms; V_1 is associated with nonbonding interactions, and V_2 is associated with hyperconjugative interactions. A natural bond orbital analysis showed that the lone pair → σ^* hyperconjugative interactions favor the gauche conformation. Furthermore, the infrared spectra for the liquid and solid phases and the Raman spectrum for the liquid have been recorded, and the observed bands have been assigned to the vibrational normal modes. The experimental vibrational data, along with calculated theoretical force constants, were used to define a scaled quantum mechanical force field for the target system that enabled us to estimate the measured frequencies with a final root-mean-square deviation of 6 cm^{-1}.

Introduction

Methanethiosulfonate reagents were first developed as tools to probe the structures and functions of proteins, particularly membrane proteins such as ion channels.[1] The reagents react selectively and rapidly with thiols (sulfhydryls) to form disulfide bonds and, therefore, are highly efficient labeling agents for cysteine residues in proteins.[2] Papers have been published describing applications of methanethiosulfonates in cancer research[3] and as chemopreventive agents for liver neoplasia when administered in combination with Phenobarbital,[4] a bio-antimutagen reagent.[5]

Despite the vast interest in these compounds, the molecular structure and vibrational characteristics of methyl methanethiosulfonate, $CH_3SO_2SCH_3$, (abbreviated MMTS) are still not known. We have, therefore, extended our investigation of different derivatives of methane-, trifluoromethane-, and trichloromethanesulfonic acids[6−10] to this substance to obtain more information about the conformational characteristics and vibrational spectrum. Methanesulfonates and methanethiosulfonates can form both anti and gauche conformers by rotating about the central O−S and S−S bonds, respectively, and their preferences for one conformer or other have been studied in the past both experimentally, mainly by NMR spectroscopy,[11] and theoretically, using ab initio calculations,[12] to determine the effects of substituent groups on O and S. The gas-phase structure of MMTS has been determined by gas-phase electron-diffraction (GED) techniques. Additionally, infrared and Raman spectra have been recorded in different physical states. These experimental measurements were complemented by quantum chemical calculations to obtain an optimized molecular structure and a scaled quantum mechanical force field. Furthermore, the barrier to internal rotation about the S−S bond has been calculated using an assortment of computational approaches (both ab initio and density functional theory (DFT)) and has been fitted to a 6-fold Fourier-type expansion. This methodology has allowed us to analyze the nature of the potential function and to assess the preferred conformation of the molecule. The study has been completed by natural bond orbital (NBO) analysis to determine the presence of hyperconjugative interactions, which would favor one conformation over another. We have compared the experimental and theoretical structures and conformations of MMTS with the experimental results previ-

* To whom correspondence should be addressed. Phone: +54-381-4311044; fax: +54-381-4248169; e-mail: altabef@fbqf.unt.edu.ar.
[†] Universidad Nacional de Tucumán.
[‡] Universidad de Jaén.
[§] Universidad Nacional de La Plata.
[||] University of Edinburgh.
[#] Members of the Carrera del Investigador Científico, CONICET, R. Argentina.

10.1021/jp073611n CCC: $37.00 © 2007 American Chemical Society
Published on Web 08/31/2007

TABLE 1: Calculated Molecular Structure Parameters for MMTS and Corresponding GED Values (Distances in pm, Angles in °)

	B3LYP	RHF	MP2			GED
	6-31G(d)	6-31G(d)	6-311G(d)	6-311G(3df,3pd)	6-311G(3df,3pd)[a]	
energy[b]	−1023.88881	−1024.78060	−1024.93463	−1025.28636	−1025.28327	
C(1)−S(5)	177.42	178.38	178.19	176.52	176.00	178.46(25)
S(5)−O(6)	143.04	146.34	144.99	143.43	143.78	143.28(11)
S(5)−O(7)	143.33	146.75	145.40	143.74	143.78	143.62(11)
S(5)−S(12)	206.49	210.10	211.34	206.92	208.75	207.47(9)
C(8)−S(12)	181.70	181.35	180.86	180.38	180.60	182.20(26)
C−H mean	108.06	109.11	108.95	108.63	108.64	108.86(34)
H−C(1)−H	110.5	110.7	110.7	111.1	111.2	109.6(5)
H−C(8)−H	109.8	109.6	109.4	109.9	110.2	108.6(5)
C−S−O(6)	107.7	107.6	108.0	108.1	109.1	109.4(3)
C−S−O(7)	107.3	106.9	107.4	107.3	109.1	108.6(3)
C(1)−S−S	105.4	104.5	102.6	104.1	99.6	102.8(6)
C(8)−S−S	101.1	99.6	98.2	98.9	93.8	100.3(6)
O−S−O	121.2	122.4	122.2	121.9	119.4	121.0(2)
S−S−O(6)	105.4	105.3	106.1	105.1	108.9	103.9(3)
S−S−O(7)	108.8	108.8	108.8	108.9	108.9	109.7(2)
C−S−S−C	82.5	83.5	83.2	81.2	180.0	80.1(25)

[a] C_s conformer. [b] Units of energy are Hartrees. Not corrected for zero-point energy. See Figure 2 for atom numbering.

ously obtained for $CF_3SO_2OCH_3$,[6] $CF_3SO_2OCF_3$,[10] and the carbonyl $FCOSSCH_3$,[13] all of which prefer gauche conformations.[6]

Experimental Section

A sample of MMTS was purchased from Sigma-Aldrich and was used without further purification.

Gas-Phase Electron Diffraction. Data were collected using the Edinburgh GED apparatus[14] using an accelerating voltage of around 40 keV (ca. 6 pm electron wavelength) on Kodak Electron Image films. Nozzle-to-film distances were determined using benzene vapor as a standard immediately after recording the diffraction patterns for MMTS. Sample and nozzle temperatures of 405 and 418 K, respectively, were used for the short nozzle-to-camera distance (95.6 mm), and those for the long nozzle-to-camera distance (259.1 mm) were 350 and 375 K. The electron-scattering patterns were converted into digital form using an Epson Expression 1680 Pro flatbed scanner and a scanning program described elsewhere.[15] Data reduction and least-squares refinements were carried out using the ed@ed program[16] employing the scattering factors of Ross et al.[17] The scale factors, *s* limits, weighting points, correlation parameters, and electron wavelengths are provided in Table S1 (Supporting Information).

IR and Raman Spectroscopy. Infrared spectra for MMTS in the liquid and solid phases were recorded in the 400−4000 cm^{-1} range using a Perkin-Elmer 1600 Fourier transform infrared (FTIR) instrument. The spectrum of the solid was obtained after depositing the substance from the vacuum line onto a KBr window maintained at about 197 K in a variable temperature RIIC (VLT-2) cell. The Raman spectrum of the liquid at room temperature was obtained with the FRA-106 accessory mounted on a Bruker IFS66 FTIR instrument, using 1064 nm light from a Nd/YAG laser for excitation.

Computational Details. The Gaussian 03 suite of programs[18] was used with the resources of the EPSRC National Service for Computational Chemistry Software[19] running on a cluster of 22 Linux Opteron nodes, where each Opteron server has twin 2.4 GHz Opteron 250 CPUs and 8 GB of memory connected with a high-speed, low-latency Myrinet network. Geometry optimizations were performed at the RHF, MP2, and DFT levels using a variety of basis sets. A starting geometry was obtained using RHF theory with a 3-21G(d) basis set[20−22] followed by a 6-31G(d) basis set.[23−25] Electron correlation was then considered using the MP2[26] approach with the 6-31G(d) and 6-311G(3df,3pd)[27−29] basis sets. DFT calculations were performed using Becke's three-parameter hybrid exchange functional[30] (B3) combined with both the Lee−Yang−Parr gradient-corrected correlation functional[31] (LYP) and the same basis sets as for the MP2 calculations. All calculations were performed using standard gradient techniques and default convergence criteria. Stationary points were assessed through energy analytical second derivatives, and zero-point energy corrections were neglected. The natural bond orbital (NBO) calculation was performed using the program NBO 3.1[32] as implemented in Gaussian 03. Atoms in molecules (AIM) analysis was also performed by AIM2000[33] package at B3LYP/6-311++G(d,p) level of theory.

The calculation of force constants for MMTS included a force field transformation, scaling, and determination of the potential energy distribution, which were performed with the program FCARTP.[34]

Results and Discussion

Theoretical Study. All geometry optimizations (RHF, MP2, and DFT with all basis sets) predicted a preferred gauche conformation, in agreement with the experimental results. Calculated geometric parameters for MMTS are listed in Table 1 along with the experimental electron-diffraction structure. As was found for the related compound $CF_3SO_2OCF_3$,[10] inclusion of extra polarization functions (beyond a single d function) is necessary to predict the bond lengths in this type of molecule accurately. The parameter most sensitive to this orbital description is the S−S bond, which was shortened by 4.4 pm upon replacing the 6-311G(d) basis set with 6-311G(3df,3pd). All bonds involving the SO_2 sulfur atom were shortened by over 1 pm, but the remaining bond lengths were relatively unchanged. An additional geometry optimization was performed with the 6-311G(d) basis on all atoms except sulfur, for which a 6-311G(3df) basis set was used. This produced a geometry close to both the experimental structure and that calculated using the 6-311G(3df,3pd) basis set, demonstrating that only the polarization of the basis set on sulfur is critical for obtaining accurate bond lengths in these types of structures.

From a chemical point of view, one of the main interests in disulfides and their oxidized derivatives has been the study of the preferred gauche conformation in contrast to similar

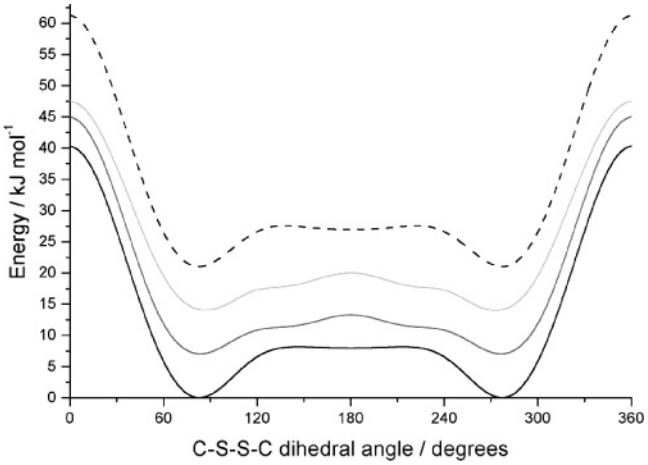

Figure 1. Torsional potential about the S−S bond in MMTS calculated in 5° increments using RHF/6-31G(d) (dashed), B3LYP/6-31G(d) (light gray), MP2/6-31G(d) (dark gray), and MP2 with a 6-31G(d) basis set on all atoms except sulfur for which a 6-31G(3df) basis set was used (black).

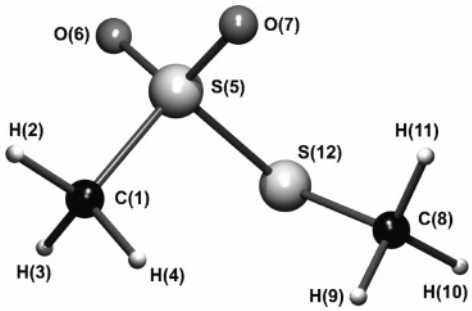

Figure 2. Molecular structure of the gauche conformer of MMTS showing atom numbering.

compounds where the anti conformer is more stable. To gain some insight into the rotational barrier of this compound, the potential energy of the C−S−S−C torsion was calculated at the RHF, MP2, and B3LYP levels using the 6-31G(d) basis set and then again at the MP2 level using a 6-31G(d) basis set on all atoms but sulfur for which a 6-31G(3df) basis set was used (Figure 1). There is good agreement between the MP2 and B3LYP methods, both identifying two minima, mirror images, with S(12)−C(8) (see Figure 2 for atom numbering) approximately eclipsing one of the S═O bonds. The RHF scan, however, predicted a third stable conformer with C_s symmetry, approximately 6 kJ mol^{-1} higher in energy than those with C_1 symmetry (Table 2). A possible origin of this C_s local minimum is the shortening of the S−S bond length predicted by RHF with respect to the values arising from MP2 and B3LYP. As mentioned above and as observed in Table 1, extra polarization functions are required in the basis set on the sulfur atoms to reproduce the experimental S−S bond length, whereas in the RHF/6-31G(d) calculation, the error introduced by the basis set deficiency is canceled by the omission of correlation energy. A second MP2 scan was therefore performed with a 6-31G-(3df) basis set on sulfur and revealed a very flat potential energy curve in the C−S−S−C range 140−220° with a shallow local minimum at 180° (Figure 1). An optimized geometry of this structure was calculated, and frequency calculations at the same level revealed only real frequencies, strengthening the argument for the presence of a metastable C_s-symmetric conformer. The difference in energy between the optimized equilibrium geometries of the C_1 and C_s conformers was calculated at this level to be 8.0 kJ mol^{-1}. However, the corresponding free-energy

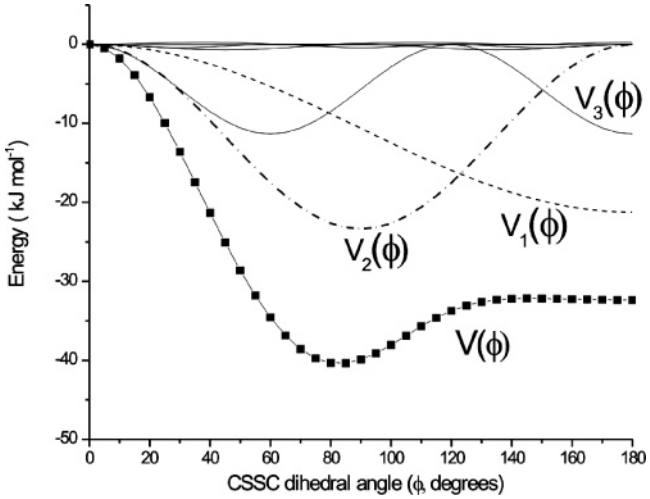

Figure 3. Fourier decomposition of potential function $V(\phi)$ for MMTS calculated using MP2 with a 6-31G(d) basis set on all atoms except sulfur for which a 6-31G(3df) basis set was used.

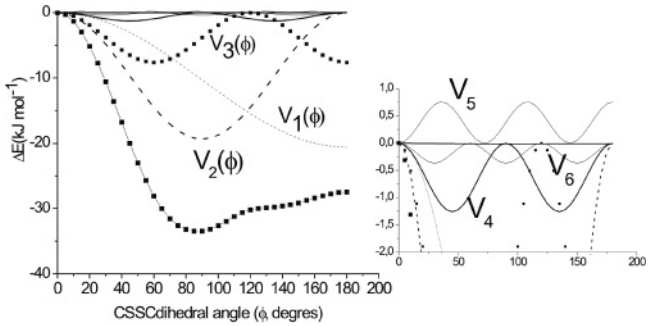

Figure 4. Fourier decomposition of potential function $V(\phi)$ for MMTS for B3LYP/6-31G(d). On the right is an enlargement of the region containing V_4, V_5, and V_6.

difference at the GED experimental temperature (ca. 400 K) was calculated to be only 1.3 kJ mol^{-1}, giving a Boltzmann population of ca. 25%. An attempt was made to confirm the presence of this conformer experimentally by adding a C_s conformer to the GED model, although because of the similarities of the radial-distribution functions of the two conformers, no useful information was obtained.

The study of the nature of the barrier to rotation of the C−S−S−C torsion in terms of hyperconjugative, steric, and electrostatic interactions will give us an insight into the reasons for the relative stability of the gauche conformer. The potential energy surface for the target torsion angle was calculated in 5° steps in the range 0−180° allowing all other geometrical parameters to relax. The energy profiles were fitted to a sixth-order Fourier expansion[35]

$$V(\theta) = \sum_{i=1}^{6} \frac{1}{2} V_{iN}(1 - \cos iN\theta) \qquad (1)$$

where N, the symmetry number, is equal to 1. No contributions to torsional energies from zero-point energy were taken into account.

The decomposition of the total energy function and the analysis of the different terms V_i has previously been shown to be an effective method of analyzing the stabilization of different conformations in molecular systems.[36−39] Table 3 lists the six V_i terms calculated for MMTS using the RHF, MP2, and B3LYP methods with the 6-31G(d) basis set. With their large values, V_1 and V_2 are the main contributions to the rotational barrier,

TABLE 2: Energy Differences between the Gauche (C_1) and Anti (C_s) Conformers of MMTS at Different Levels of Theory[a]

conformer	B3LYP/6-31G(d)	RHF/6-31G(d)	MP2/6-31G(d)	MP2/6-311G(3df,3pd)
C_1	−1026.58761	−1023.89111	−1024.78060	−1025.28636
C_s	−1026.58529	−1023.88881	−1024.77818	−1025.28327
ΔE/kJ mol^{-1}	6.1	6.0	6.3	8.1

[a] Absolute energies are in Hartrees. Not corrected for zero-point energy.

TABLE 3: Fourier Expansion Parameters/kJ mol^{-1} for MMTS

	B3LYP/6-31G(d)	RHF/6-31G(d)	MP2/[a]
V_1	−17.78	−19.83	−21.21
V_2	−18.66	−21.00	−23.30
V_3	−8.99	−13.22	−11.30
V_4	−2.89	−3.18	−0.67
V_5	0.13	−0.63	0.21
V_6	−0.75	−0.92	−0.38

[a] 6-31G(d) on all atoms except sulfur for which a 6-31G(3df) basis set was used.

with $V_2 > V_1 > V_3$. V_{4-6} are less significant when deconvoluting the potential energy curve. The magnitudes and signs of the two main terms are similar regardless of the level of theory used to calculate them. V_2 is usually associated with conjugative and hyperconjugative effects that have a periodicity of 180°. As for V_1, it usually accounts for interactions between local dipoles and for steric interactions. The V_3 term is associated with unfavorable bond−bond eclipsing interactions, exhibiting a 3-fold periodicity for a torsion involving sp^3-hybridized sulfur atoms.[37]

Figure 3 shows the Fourier decomposition for the potential energy function calculated at the MP2 level of theory with the 6-31G(3df) basis set on sulfur and the 6-31G(d) basis set on the remaining atoms. V_1 is large and negative showing that there is a strong preference for an anti geometry. This fact can be rationalized by considering the interactions between the local dipole through the SO_2Me group and that through SMe. As shown in Table 4, the overall dipole moment (μ) for the anti conformer is smaller than that for the gauche conformer indicating that in the anti conformer these local dipoles are opposite in direction, consistent with the value for V_1 given by the Fourier analysis. An attempt was made to verify this prediction by calculating Mulliken and natural population analysis (NPA)[40] charges, which are also shown in Table 4. As atomic charges are not a quantum mechanical observable, these calculated values should be treated with a great deal of caution. It is evident that the Mulliken charges are highly unpredictable, especially with respect to basis set, and that the values predicted are unrealistic even with the largest basis set. The NPA charges show more consistency but predict a local dipole on SMe in the opposite direction to that anticipated by the Fourier analysis and the molecular dipole moments, μ. Therefore, it remains unclear whether or not the V_1 term can be explained by interactions between pairs of local dipoles for this compound.

As with the V_1 term, V_3 also preferentially stabilizes the anti conformer, but the large and negative V_2 term favors the gauche form over the anti conformer. The balance between V_1, V_2, and V_3 leads to the flat region in the potential curve between 130° and 180°. Figure 4 shows the Fourier decomposition calculated using B3LYP/6-31G(d), where such a flat region is not present and the anti conformer is predicted to be unstable. Table 3 shows that the value of the V_3 term is 2.3 kJ mol^{-1} smaller for this potential energy curve than for the MP2 curve shown in Figure 3, suggesting that the predicted steric eclipsing interactions are much weaker. As a longer S−S bond would reduce the repulsive steric interactions, this finding is consistent with the overestimation of the S−S bond length at this level of theory, uncovered by the GED analysis.

To summarize the Fourier analysis, V_1 and V_2 are the dominant terms and are comparable in magnitude. However, V_2 is the more important for determining which conformer is most stable as it stabilizes the gauche conformer without stabilizing the anti conformer. Although the V_3 term is unimportant in terms of determining which conformer is the more stable, it is largely responsible for the shape of the potential energy curve in the flatter region. Since V_2 is the most important term of the Fourier expansion, it can be inferred that hyperconjugative effects are more important than steric or electrostatic interactions in predicting the lowest-energy structure.

The role of hyperconjugative interactions in the stabilization of the gauche conformer has been assessed using NBO analysis, where the hyperconjugation represents the transfer of an electron between a lone pair or bonding orbital and an antibonding orbital. Table 5 contains the main hyperconjugative interactions for the gauche and anti forms of MMTS. In terms of the NBO analysis, hyperconjugation interactions are more favored in the gauche conformation than in the anti one. Thus, lone pairs of the oxygen and sulfur atoms transfer electronic charge to the antibonding σ^* orbital of the C−S and S═O bonds and these stabilizing interactions are stronger for the gauche form. A comparative study of the skeleton internal barrier and the corresponding NBO analysis for this family of compounds has been done by the authors and will be the subject of another paper to be published.

One final attempt was made to rationalize the composition of MMTS. Bader's atoms in molecules theory[41] (AIM) predicts a stabilizing intramolecular contact involving a H(11) and an O(6). This interaction is not supported by the NBO analysis provided no second-order perturbation contributions are found. Since the default output for NBO 3.1 code reports only those second-order terms achieving a threshold of around 1 kJ mol^{-1} for intramolecular interactions, we consider that the target contact is very weak and that it does not modify the conclusions already outlined. One should bear in mind the fact that the sum of the second-order contributions reported in Table 5 favors the gauche conformation over the anti one by approximately 16 kJ mol^{-1}.

GED Study. The molecular model for the GED refinement was assigned overall C_1 symmetry as predicted by the ab initio calculations (Tables S2 and S3, Supporting Information). (The atom numbering used in the model and calculations is shown in Figure 2.) The structure of MMTS was defined in terms of 19 independent parameters, comprising six bond lengths and differences, eight bond angles and differences, two tilt angles, and three torsional angles.

The bonded S−S distance was defined individually (p_2) and, on the basis of the ab initio calculations and the low scattering ability of hydrogen, the six C−H bonds were assumed to be of equal length (p_1). The S═O bond lengths were defined in terms of the average (p_5) and difference [S═O(7) minus S═O(6), p_6] as were the two C−S bonds [p_3 is the average and p_4 is defined as C(8)−S(12) minus C(1)−S(5)].

TABLE 4: Atomic Charges and Dipole Moments (μ) for MMTS Calculated with (a) the Mulliken Theory and (b) the NPA Theory Using Different Methods

	gauche ϕ((CSSC) = 80.1°[a]						anti f ((CSSC) = 180.0°					
	RHF/6-31G(d)		MP2/6-31G(d)		B3LYP/6-31G(d)		HF/6-31G(d)		MP2/6-31G(d)		B3LYP/6-31G(d)	
	(a)	(b)	(a)	(b)	(a)	(b)	(a)	(b)	(a)	(b)	(a)	(b)
$C(1)H_3$	−0.007	−0.120	0.003	−0.110	0.017	−0.130	−0.013	−0.113	−0.005	−0.100	0.026	−0.100
S(5)	1.283	2.254	1.294	2.205	0.959	2.067	1.273	2.246	1.284	2.192	0.943	1.989
O(6)	−0.654	−1.047	−0.683	−1.045	−0.513	−0.938	−0.659	−1.054	−0.674	−1.039	−0.504	−0.917
O(7)	−0.665	−1.058	−0.669	−1.034	−0.503	−0.947	−0.659	−1.054	−0.674	−1.039	−0.504	−0.917
S(12)	0.038	0.023	0.053	0.039	0.018	0.009	0.034	0.003	0.053	0.022	0.016	−0.014
$C(8)H_3$	0.005	−0.050	0.003	−0.050	0.008	−0.060	0.020	−0.027	0.016	−0.03 5	0.023	−0.040
μ/Debye	5.072	5.072	5.138	5.138	4.360	4.360	3.108	3.108	3.250	3.250	2.510	2.510

[a] GED value.

TABLE 5: Important Hyperconjugative Interactions (kJ mol^{-1}) for MNTS Calculated Using the B3LYP/ 6-311++G(d,p) Method[a]

	gauche ϕ (CSSC) = 86.4°	anti ϕ (CSSC) = 180.0°
LP S(12) → σ* C(1)−S(5)	12.13	
LP S(12) → σ* S(5)═O(6)	9.20	6.52
LP S(12) → σ* S(5)═O(7)	2.93	6.52
LP O(6) → σ* S(5)−S(12)	109.60	106.70
LP O(6) → σ* S(5)═O(7)	37.24	38.91
LP O(6) → σ* C(1)−S(5)	69.90	50.21
LP O(7) → σ* S(5)−S(12)	83.30	106.70
LP O(7) → σ* C(1)−S(5)	71.90	50.21
LP O(7) → σ* S(5)═O(6)	24.27	38.91
total	420.50	404.70

[a] LP is a lone pair on the specified atom.

The geometry of the sulfonyl group in relation to C(1) and S(12) was described using the S−S−C(1) angle (p_7), the average of the two S−S═O angles (p_8) in combination with their difference [S−S═O(7) minus S−S═O(6), p_9], and the average of the two C−S═O angles (p_{10}) combined with their difference [C−S═O(6) minus C−S═O(7), p_{11}].

Local C_3 symmetry was assumed for both methyl groups. Separate internal H−C−H angles were used for each methyl group. These were defined in terms of the average H−C−H angle (p_{13}) and the difference (p_{14}) between the averages for the two groups [H−C(1)−H minus H−C(8)−H]. The methyl group containing C(1) was oriented with respect to the rest of the molecule using a tilt angle (p_{15}, defined as the angle between the local C_3 axis and the C−S bond with a reduction in the S−C−H(2) angle being positive) and the S−S−C−H(2) torsion (p_{18}). The positioning of C(8) was performed using a second S−S−C angle (p_{12}) and the C−S−S−C torsion (p_{17}). Finally, hydrogen atoms 9−11 were positioned using a second tilt angle (p_{16}, defined as above with a reduction of the S−C−H(10) angle being positive) and the S−S−C−H(10) angle (p_{19}). As an internal H−C−H angle was used for each methyl group, these angles were unaffected by application of the torsion or tilt angles.

A second GED refinement was performed using a two-conformer model. However, the radial-distribution functions for the two conformers are so similar that either conformer or any mixture of conformers fitted the data equally well. Therefore, only the single-conformer (C_1) refinement is presented.

The GED refinement was carried out using the SARACEN method,[42] which allows parameters to be restrained to calculated values with specified uncertainties, on the basis of the degree

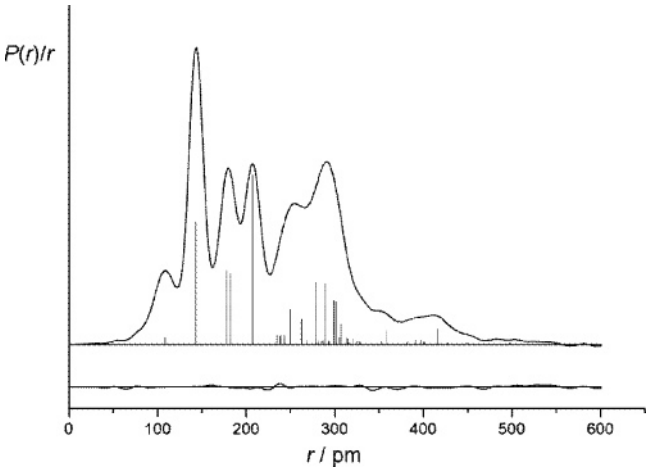

Figure 5. Experimental and difference (experimental minus theoretical) radial-distribution curves, $P(r)/r$, for MMTS. Before Fourier inversion, the data were multiplied by s: $\exp[(-0.00002s^2)/(Z_S - f_S)^2]$.

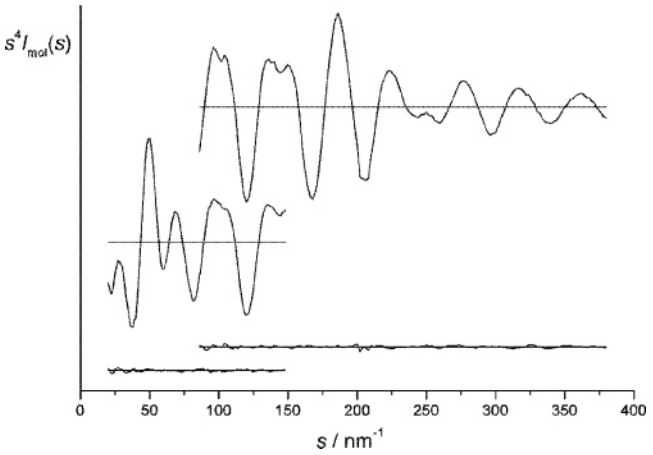

Figure 6. Experimental and weighted difference (experimental minus theoretical) molecular-scattering intensity curves for $CH_3SO_2SCH_3$.

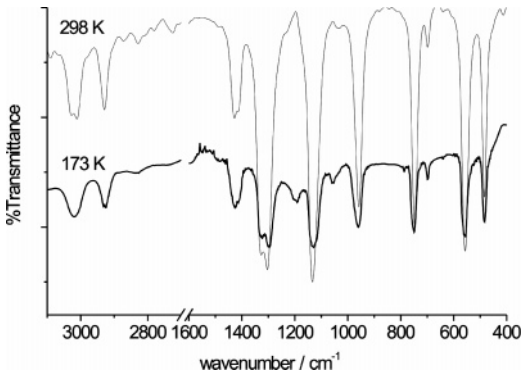

Figure 7. Infrared spectra of MMTS in the liquid phase (upper trace; resolution 2 cm^{-1}) and in the solid phase (lower trace; thin layer on KBr window; resolution 2 cm^{-1}).

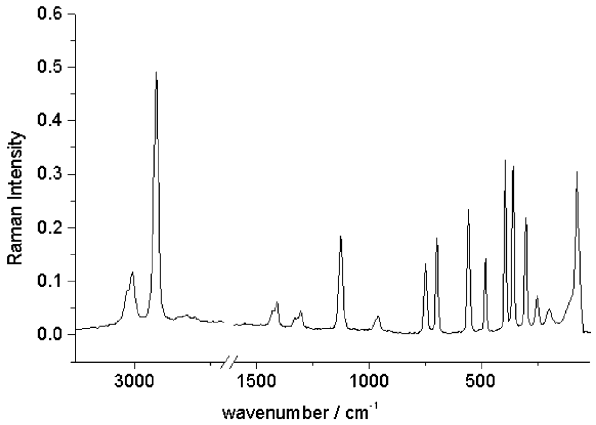

Figure 8. Raman spectrum of liquid MMTS; resolution 4 cm^{-1}.

of convergence of the calculations. All 19 independent parameters were refined, along with one individual and seven groups of amplitudes of vibration, producing an R_G factor of 0.081 (R_D = 0.048). The force field obtained at the MP2/6-31G(d) level was then used by the program SHRINK[43] to obtain estimates of the amplitudes of vibration (u_{h1}) and perpendicular vibrational correction terms (k_{h1}) used in the GED refinement. The refined parameters are displayed in Table 6 along with the corresponding values predicted by MP2/6-311G(3df,3pd) calculations. The radial-distribution and molecular-intensity scattering curves are shown in Figures 5 and 6, respectively.

Restraints on geometrical parameters were derived from the MP2/6-311G(3df,3pd) calculated values. Those applied directly to independent or dependent parameters are listed in Table 6. A full list of interatomic distances and corresponding amplitudes of vibration is given in Table S4 (Supporting Information). The amplitude of vibration for the S−S bond was refined individually as this was the only distance comprising heavy atoms contributing to the corresponding peak in the radial-distribution curve (Figure 5). Seven groups of amplitudes, corresponding to the remaining peaks in the radial-distribution curve, were also refined. Those amplitudes corresponding to nonbonded distances were restrained with uncertainties of 10% of their calculated values, as were the group of amplitudes for the bonded C−S distances. The least-squares correlation matrix (Table S5, Supporting Information) shows all parameters with greater than 50% correlation.

Vibrational Study. The major conformer of MMTS has C_1 symmetry, and its 30 normal modes of vibration are active in both the IR and Raman spectra. Representative spectra appear in Figures 7 (IR spectra of the liquid and solid phases) and 8- (Raman spectrum of the liquid), and the frequencies of the observed spectral features appear in Table S6 (Supporting Information). The calculations were based in these condensed state data because the low vapor pressure of the substance prevented the collection of gas-phase frequencies more appropriate for comparison with the theoretical frequencies.

The DFT calculations carried out with the B3LYP/6-31G(d) combination of functional and basis set reproduced the normal frequencies of vibration with a root-mean-square deviation (rmsd) of 79 cm^{-1}. These calculated frequencies were used for the vibrational analysis to allow comparison of the present results with those obtained for related molecules. In addition, the B3LYP/6-31G(d) approach has previously been extensively used for vibrational calculations as a good compromise between economy of computational resources, accuracy, and applicability to many-atoms systems.[6−10] The selected experimental and the calculated frequencies of vibration are reported in Table 7. The assignments of spectral features to the different modes of vibration (Tables 7 and S6, Supporting Information) are based on the calculated frequencies, the infrared and Raman intensities, and the comparison with known data for related molecules.

Methyl Modes. Three well-defined bands can be observed in the 3100−2900 cm^{-1} region and are assigned to the six CH_3 stretching modes. The strongest band in the Raman spectrum, at 2929 cm^{-1}, has a strong counterpart in the IR spectrum, split into two components at 2931 and 2924 cm^{-1} at low temperature. These features are assigned to the symmetric stretching modes of the two methyl groups. The symmetric CH_3 stretching modes in CH_3SO_2OH[44] and CCl_3SCH_3[45] appear at 2942 and 2926 cm^{-1}, respectively.

The bands at 3027 and 3010 cm^{-1} are due to the four antisymmetric CH_3 stretching modes. The first one is assigned to the ν_2 and ν_3 modes, predicted at almost the same frequency by the calculations (Table 7), whereas the second band is assigned to ν_4. No band was observed that could be assigned to the remaining stretching mode, ν_1.

The six deformation modes of the CH_3 groups should appear in the 1500−1300 cm^{-1} region, where two groups of bands are observed. The first group, located between 1480 and 1380 cm^{-1}, corresponds to the four antisymmetric CH_3 deformation modes, although only three bands can be discerned in the spectra. The location of these features are in agreement with the calculated frequencies for the ν_9 and ν_{10} modes (Table 7). The two symmetric CH_3 deformation modes appear close together as a strong infrared band, centered at 1327 cm^{-1}, which partially overlaps the strong SO_2 stretching band at 1304 cm^{-1}.

The strong band at 958 cm^{-1}, flanked by shoulders in the IR and Raman spectra, is assigned to the four rocking modes of the CH_3 groups. This is in accordance with the close-lying frequencies predicted by the calculations for these modes (Table 7).

SO_2 Modes. Two strong infrared bands, at 1304 and 1133 cm^{-1}, are assigned to the SO_2 antisymmetric and symmetric stretching modes, respectively. The first value is considerably lower than the corresponding one measured for $CF_3SO_2OCF_3$ (1469 cm^{-1}).[10] A comparable shift of the antisymmetric mode in the hydrogenated molecule was also observed on going from $CF_3SO_2OCH_2CF_3$ (1448 cm^{-1})[7] to $CH_3SO_2OCH_2CH_3$ (1350 cm^{-1}).[9]

The medium-intensity band located at 483 cm^{-1} in the infrared and Raman spectra is assigned to the SO_2 bending mode. It is strongly mixed with the C(1)−S stretching and the SO_2 wagging modes. The low-frequency modes corresponding to the vibrations of the whole SO_2 group appear at 557 cm^{-1} (SO_2 wagging), 394 cm^{-1} (SO_2 rocking), and 304 cm^{-1} (SO_2 twisting). These assignments are supported by the corresponding measured frequencies for the CF_3SO_2X molecules[46] and by the present calculations.

Skeletal Modes. The S−S stretch, which is strongly mixed with the SO_2 wagging and rocking modes, appears as a main component of the ν_{21}, ν_{23}, and ν_{24} modes, associated with strong Raman bands at 557, 394, and 360 cm^{-1}. The first band is not far from that assigned to the S−S stretching in $FC(O)SSCH_3$, located at 537 cm^{-1}.[47]

The C(1)−S and C(8)−S stretching modes are associated with the bands located at 748 and 698 cm^{-1}, respectively, in the infrared and Raman spectra. The deformations of the angles between these bonds and the S−S bond cause the weak Raman bands at 253 and 200 cm^{-1}, respectively.

Torsional Modes. There are three torsional modes, which should have low frequencies. In accordance with the theoretical

TABLE 6: GED Refined Parameters for MMTS (Distances in pm, Angles in °)

independent parameter	description	GED value	MP2/6-311G(3df,3pd)[a]
p_1	rC−H	108.86(34)	108.63
p_2	rS−S	207.47(9)	206.92
p_3	rC−S mean	180.33(10)	178.45
p_4	rC(8)−S(12) minus C(1)−S(5)	3.74(47)	3.86(50)
p_5	rSO mean	143.45(4)	143.59
p_6	rS−O(7) minus S−O(6)	0.34(19)	0.31(20)
p_7	∠S−S−C(1)	102.8(6)	104.1
p_8	∠S−S−O mean	106.8(2)	107.0
p_9	∠S−S−O(7) minus S−S−O(6)	5.8(3)	3.8(10)
p_{10}	∠C−S−O mean	109.0(2)	107.7
p_{11}	∠C−S−O(6) minus C−S−O(7)	0.8(5)	0.8(5)
p_{12}	∠S−S−C(8)	100.3(6)	98.9
p_{13}	∠H−C−H mean	109.1(5)	110.5(10)
p_{14}	∠H−C(1)−H minus H−C(8)−H	0.9(5)	1.1(5)
p_{15}	∠Me C(1) tilt	1.5(9)	1.6(10)
p_{16}	∠Me C(8) tilt	1.9(9)	2.5(10)
p_{17}	ϕC−S−S−C	279.9(25)	278.8
p_{18}	ϕS−S−C−H(2)	179.6(19)	179.7(20)
p_{19}	ϕS−S−C−H(10)	190.3(43)	191.1(50)
	Dependent Parameter		
d_1	∠O−S−O	121.0(2)	121.9(4)
d_2	∠S−S−C(1) minus S−S−C(8)	2.5(11)	5.2(20)
d_3	∠C−S−O minus S−S−O ($p_{10} - p_8$)	2.1(3)	0.7(10)

[a] Where calculated values are followed by a number in parentheses, a restraint was applied to the corresponding parameter using the calculated value. The numbers in parentheses are the uncertainties of the restraints.

TABLE 7: Observed and Calculated Frequencies, Infrared and Raman Intensities, and Potential Energy Distribution for MMTS

mode	observed	calculated[a]	calc. SQM[b]	IR intensities[c]	Raman activity[d]	potential energy distribution (≥10%)[e]	approximate description of mode
1		3202	3046	0.39	44.9	96 S_1	ν_{as} C(1)H_3
2	3027	3183	3029	0.34	80.8	95 S_2	ν_{as} C(1)H_3
3	3027	3181	3027	1.46	37.2	78 S_3 + 20 S_4	ν_{as} C(8)H_3
4	3011	3160	3007	5.28	88.6	21 S_3 + 80 S_4	ν_{as} C(8)H_3
5	2931	3085	2935	0.26	109.6	99 S_5	ν_s C(1)H_3
6	2924	3074	2924	13.2	125.7	99 S_6	ν_s C(8)H_3
7	1428	1509	1435	13.56	11.7	93 S_7	δ_{as} C(8)H_3
8	1414	1494	1419	11.43	20.3	90 S_8	δ_{as} C(8)H_3
9	1409	1481	1405	3.25	10.6	94 S_9	δ_{as} C(1)H_3
10	1409	1480	1404	7.18	14.9	91 S_{10}	δ_{as} C(1)H_3
11	1327	1387	1334	12.86	5.1	83 S_{11} + 15 S_{13}	δ_s C(8)H_3
12	1327	1374	1321	10.06	0.9	99 S_{12}	δ_s C(1)H_3
13	1304	1329	1301	155.92	6.1	20 S_{11} + 77 S_{13}	ν_{as} SO_2
14	1131	1118	1133	163.28	12.0	92 S_{14}	ν_s SO_2
15	983	1002	980	6.51	4.14	89 S_{15}	ρ C(8)H_3
16	972	1001	975	2.25	6.4	73 S_{16}	ρ C(8)H_3
17	958	991	958	35.19	5.5	73 S_{17}	ρ C(1)H_3
18	958	987	953	4.58	7.6	10 S_{16} + 70 S_{18}	ρ C(1)H_3
19	748	725	740	74.68	12.2	73 S_{19} + 21 S_{23}	ν C(1)S(5)
20	698	699	703	2.05	10.2	100 S_{20}	ν S(12)C(8)
21	557	527	565	104.57	10.3	30 S_{21} + 45 S_{22} + 24 S_{23}	ν S(5)S(12)
22	483	457	486	36.15	8.7	21 S_{19} + 41 S_{22} + 32 S_{23}	w SO_2
23	394	373	397	0.47	7.8	10 S_{23} + 39 S_{24} + 18 S_{28}	δ SO_2
24	360	327	353	0.49	13.9	12 S_{18} + 37 S_{21} + 10 S_{23} + 40 S_{24}	ρ SO_2
25	304	277	297	0.01	8.9	81 S_{25}	tw SO_2
26	253	227	253	1.74	0.9	100 S_{26}	τ C(1)S(5)S(12)
27	253	223	249	0.74	1.4	92 S_{27}	τ C(1)H_3
28	200	189	199	1.17	1.1	20 S_{24} + 61 S_{28}	δ S(5)S(12)C(8)
29	114	111	123	0.45	0.3	100 S_{29}	τ C(8)H_3
30	76	64	71	3.07	1.1	100 S_{30}	τ S−S
RMSD (cm^{-1})		79	6				

[a] B3LYP/6-31G* calculation. Observed and calculated values in cm^{-1}. [b] From scaled quantum mechanics force field (see text). [c] Units are km mol^{-1}. [d] Units are $Å^4$ $(amu)^{-1}$. [e] Coordinate numbers correspond to Table S4 (Supporting Information).

calculations, the weak Raman bands located at 253 and 114 cm^{-1} can be assigned to the torsional vibrations of the C(1)H_3 and C(8)H_3 methyl groups, respectively, whereas the torsion around the S−S bond is assigned to the lowest observed band at approximately 76 cm^{-1}.

Calculation of Force Constants. The B3LYP/6-31G(d) Cartesian force field was transformed to the set of nonredundant, natural coordinates defined in Table S7 (Supporting Information). Such coordinates take into account the local symmetry around the C and S atoms and follow the proposals of Fogarasi

TABLE 8: Force Constants in Internal (Valence) Coordinates for $CH_3SO_2SCH_3$ and Related Molecules

force constant[a]	$CH_3SO_2SCH_3$[b]	$CH_3SO_2OCH_2CH_3$[c]	CH_3SO_2OH[d]	$CH_3SO_2OCH_3$[e]
f(C−H) (C(1)H_3)	4.96	4.96	4.91	4.95
f(C−H) (C(8)H_3)	4.91	4.90		4.74
f(C(1)−S)	2.99	3.74	3.47	3.55
f(S−X)	2.23	4.08	4.31	4.30
f(S═O)	9.24	9.82	10.2	9.73
f(C(8)−X)	3.08	4.13		4.43
f(O═S═O)	1.23	1.26	1.35	1.36
f(X−S═O)	1.39	1.31	1.41	1.41
f(C(1)−S−X)	1.05	1.29	1.31	1.39
f(C(1)−SdO)	1.14	1.10	1.21	1.18
f(X−C(8)−H)	0.52	0.68		0.58
f(H−C(1)−H)	0.42	0.43	0.43	0.42
f(H−C(8)−H)	0.44	0.45	0.42	0.46
f(S−X−C(8))	1.21	0.833		1.15
f(S═O/S═O)	0.20	0.0035		0.0026
f(C−H/C−H)	0.028	0.027		0.024

[a] Units are mdyn $Å^{-1}$ for stretches and stretch/stretch interactions and mdyn Å rad^{-2} for angle bends. [b] This work. [c] Reference 9. [d] Reference 44. [e] Unpublished results.

et al.[48] The resulting force field was subsequently scaled using the scheme proposed by Pulay et al.,[49] where the diagonal force constants are multiplied by a set of scale factors k_i, k_j, ... and the corresponding interaction constants are multiplied by $(k_i \times k_j)^{1/2}$. A set of initial scale factors was defined using the values recommended by Kalincsák and Pongor[50] where available and using unity for the remaining ones. These scale factors were subsequently fitted by a least-squares procedure to obtain the best fit to the experimental frequencies. (Initial and final scale factors are available in Table S8, Supporting Information.) All vibrational bands were assigned the same weight in the adjustment except for those missing or showing uncertain frequencies; in these cases, a value of zero was used. No empirical correction of the theoretical geometry was used. The potential energy distribution matrix was calculated with the resulting scaled quantum mechanics (SQM) force field. The final rmsd and potential energy distribution are presented in Table 7.

The SQM force field (Table S9, Supporting Information) was used to calculate the internal force constants shown in Table 8. They are compared with equivalent values for related molecules. It can be seen that the force constants corresponding to internal coordinates comprising the two bonded S atoms in CH_3SO_2-SCH_3 have lower values than those calculated for the other molecules. This can be explained by the higher mass and larger atomic radius of the sulfur atom.

Conclusions

A complete investigation of the gas-phase molecular structure of MMTS was carried out using electron-diffraction techniques complemented by theoretical methods. The experimental structure shows that this molecule is present mainly as a gauche conformer having a C−S−S−C dihedral angle of 80.1(25)°, very close to the 81−87° range of values predicted by quantum chemical calculations. A second conformer having a plane of symmetry (C_s point group) is apparent in the scan of the potential energy surface associated with the C−S−S−C torsion angle at the RHF level and is confirmed by MP2 calculations using a 6-31G(3df) basis set on sulfur and a 6-31G(d) basis set on the remaining atoms. This C_s conformer is located 8.0 kJ mol^{-1} higher than the most stable, gauche conformer. These results are in agreement with what seem to be common structural characteristics of covalent sulfonates. The decomposition of the potential energy function as a Fourier expansion and the analysis of the different terms (V_i) has shown to be useful in analyzing the relative stabilities of different conformations of molecular systems. Since V_2 is the main term of the Fourier expansion, it is concluded that the hyperconjugative effects, rather than the steric or repulsive interactions, are the driving force for the observed composition.

The role of hyperconjugative interactions in the stabilization of the gauche form has been assessed by NBO analysis, where the hyperconjugation represents an electron transfer between lone pairs or bonding orbitals and antibonding orbitals.

IR and Raman spectra were obtained for MMTS, in which bands assignable to 29 out of the expected 30 normal modes of vibration were observed. The vibrational data were used as a basis to define an SQM force field and internal force constants for MMTS.

Acknowledgment. The research grants of CIUNT (Consejo de Investigaciones de la Universidad Nacional de Tucumán), CONICET (Consejo Nacional de Investigaciones Científicas y Técnicas, PIP 6457), ANPCYT (Agencia Nacional de Promoción Científica y Tecnológica, BID 1728/OC-AR, PICT 11127), UNLP (Universidad Nacional de La Plata), and EPSRC (Grant EP/C513649) are gratefully acknowledged.

Supporting Information Available: Detailed information is available on the electron-diffraction experiment (Table S1), Cartesian coordinates related to the GED refined structure (Table S2) and to the MP2/6-311G(3df,3pd) calculated structure (Table S3), interatomic distances and related amplitudes of vibration (Table S4), least-squares correlation matrix (Table S5), frequencies of observed bands in the infrared and Raman spectra of MMTS (Table S6), definitions of the local symmetry coordinates used (Table S7), scaling factors for force constants (Table S8), and the SQM force field matrix (Table S9). This material is available free of charge via the Internet at http://pubs.acs.org.

References and Notes

(1) Fahlke, C.; Rhodes, T. H.; Desai, R. R.; George, A. L., Jr. *Nature* **1998**, *394*, 687.

(2) St-Vincent, M.; Dickman, M. *J. Chem. Educ.* **2004**, *81*, 1048.

(3) Mori, H.; Matsunaga, K.; Tanakamaru, Y.; Kawabata, K.; Yamada, Y.; Sugie, S.; Nishikawa, A. *Cancer Lett.* **1999**, *135*, 123.

(4) Surqui, S.; Okamoto, K.; Ohnishi, M.; Makito, H.; Kawamori, T.; Watanake, T.; Tamaka, T.; Nakamura, Y. K.; Nakamura, Y.; Tomito, I.; Mori, H. *J. Cancer Res.* **1997**, *88*, 5.

(5) Nakamura, Y. K.; Matsuo, T.; Simio, K.; Nakamura, Y.; Tomita, I. *Biosci., Biotechnol., Biochem.* **1996**, *60*, 1439.

(6) Trautner, F.; Ben Altabef, A.; Fernández, L. E.; Varetti, E. L.; Oberhammer, H. *Inorg. Chem.* **1999**, *38*, 3051.
(7) Tuttolomondo, M. E.; Fernández, L. E.; Navarro, A.; Varetti, E. L.; Ben Altabef, A. *Spectrochim. Acta, Part A* **2004**, *60*, 611.
(8) Tuttolomondo, M. E.; Navarro, A.; Varetti, E. L.; Ben Altabef, A. *Spectrochim. Acta, Part A* **2005**, *61*, 1011.
(9) Tuttolomondo, M. E.; Navarro, A.; Peña, T.; Varetti, E. L.; Ben Altabef, A. *J. Phys. Chem. A* **2005**, *109*, 7946.
(10) Tuttolomondo, M. E.; Argañaraz, P. E.; Varetti, E. L.; Hayes, S. A.; Wann, D. A.; Robertson, H. E.; Rankin, D. W. H.; Ben Altabef, A. *Eur. J. Inorg. Chem.* **2007**, 1381.
(11) Freeman, F.; Angeletakis, C. N. *J. Org. Chem.* **1982**, *47*, 4194.
(12) Raabe, G; Gais, H.-J.; Fleischhauer, J. *J. Am. Chem. Soc.* **1996**, *118*, 4622.
(13) Erben, M. F.; Della Védova, C. O. *Helv. Chim. Acta* **2003**, *86*, 2379.
(14) Huntley, C. M.; Laurenson, G. S.; Rankin, D. W. H. *J. Chem. Soc., Dalton Trans.* **1980**, 954.
(15) Fleischer, H.; Wann, D. A.; Hinchley, S. L.; Borisenko, K. B.; Lewis, J. R.; Mawhorter, R. J.; Robertson, H. E.; Rankin, D. W. H. *Dalton Trans.* **2005**, 3221.
(16) Hinchley, S. L.; Robertson, H. E.; Borisenko, K. B.; Turner, A. R.; Johnston, B. F.; Rankin, D. W. H.; Ahmadian, M.; Jones, J. N.; Cowley, A. H. *Dalton Trans.* **2004**, 2469.
(17) Ross, A. W.; Fink, M.; Hilderbrandt, R. In *International Tables for Crystallography*; Wilson, A. J. C., Ed.; Kluwer Academic Publishers: Dordrecht, The Netherlands, 1992; Vol. C, p 245.
(18) Frisch, M. J.; Trucks, G. W.; Schlegel, H. B.; Scuseria, G. E.; Robb, M. A.; Cheeseman, J. R.; Montgomery, J. A., Jr.; Vreven, T.; Kudin, K. N.; Burant, J. C.; Millam, J. M.; Iyengar, S. S.; Tomasi, J.; Barone, V.; Mennucci, B.; Cossi, M.; Scalmani, G.; Rega, N.; Petersson, G. A.; Nakatsuji, H.; Hada, M.; Ehara, M.; Toyota, K.; Fukuda, R.; Hasegawa, J.; Ishida, M.; Nakajima, T.; Honda, Y.; Kitao, O.; Nakai, H.; Klene, M.; Li, X.; Knox, J. E.; Hratchian, H. P.; Cross, J. B.; Bakken, V.; Adamo, C.; Jaramillo, J.; Gomperts, R.; Stratmann, R. E.; Yazyev, O.; Austin, A. J.; Cammi, R.; Pomelli, C.; Ochterski, J. W.; Ayala, P. Y.; Morokuma, K.; Voth, G. A.; Salvador, P.; Dannenberg, J. J.; Zakrzewski, V. G.; Dapprich, S.; Daniels, A. D.; Strain, M. C.; Farkas, O.; Malick, D. K.; Rabuck, A. D.; Raghavachari, K.; Foresman, J. B.; Ortiz, J. V.; Cui, Q.; Baboul, A. G.; Clifford, S.; Cioslowski, J.; Stefanov, B. B.; Liu, G.; Liashenko, A.; Piskorz, P.; Komaromi, I.; Martin, R. L.; Fox, D. J.; Keith, T.; Al-Laham, M. A.; Peng, C. Y.; Nanayakkara, A.; Challacombe, M.; Gill, P. M. W.; Johnson, B.; Chen, W.; Wong, M. W.; Gonzalez, C.; Pople, J. A. *Gaussian 03*, Revision C.01; Gaussian, Inc.: Wallingford, CT, 2004.
(19) EPSRC National Service for Computational Chemistry Software. http://www.nsccs.ac.uk.
(20) Binkley, J. S.; Pople, J. A.; Hehre, W. J. *J. Am. Chem. Soc.* **1980**, *102*, 939.
(21) Gordon, M. S.; Binkley, J. S.; Pople, J. A.; Pietro, W. J.; Hehre, W. J. *J. Am. Chem. Soc.* **1982**, *104*, 2797.
(22) Pietro, W. J.; Francl, M. M.; Hehre, W. J.; DeFrees, D. J.; Pople, J. A.; Binkley, J. S. *J. Am. Chem. Soc.* **1982**, *104*, 5039.
(23) Hehre, W. J.; Ditchfield, R.; Pople, J. A. *J. Chem. Phys.* **1972**, *56*, 2257.
(24) Hariharan, P. C.; Pople, J. A. *Theor. Chim. Acta* **1973**, *28*, 213.
(25) Gordon, M. S. *Chem. Phys. Lett.* **1980**, *76*, 163.
(26) Møller, C.; Plesset, M. S. *Phys. Rev.* **1934**, *46*, 618.
(27) McLean, A. D.; Chandler, G. S. *J. Chem. Phys.* **1980**, *72*, 5639.
(28) Krishnan, R.; Binkley, J. S.; Seeger, R.; Pople, J. A. *J. Chem. Phys.* **1980**, *72*, 650.
(29) Frisch, M. J.; Pople, J. A.; Binkley, J. S. *J. Chem. Phys.* **1984**, *80*, 3265.
(30) Becke, A. D. J. *Chem. Phys.* **1993**, *98*, 5648.
(31) Lee, C.; Yang, W.; Parr, R. G. *Phys. Rev. B* **1988**, *37*, 785.
(32) Glendening, E. D.; Badenhoop, J. K.; Reed, A. D.; Carpenter, J. E., Weinhold, F. F. Theoretical Chemistry Institute, University of Wisconsin, Madison, WI, 1996.
(33) Biegler-Köning, F.; Schönbohm, J.; Bayles, D. *J. Comput. Chem.* **2001**, *22*, 545.
(34) Collier, W. B. Program FCARTP (QCPE # 631); Department of Chemistry, Oral Roberts University: Tulsa, OK, 1992.
(35) Pitzer, R. M.; Lipscomb, W. N. *J. Chem. Phys.* **1963**, *39*, 1995.
(36) Radom, L.; Pople, J. A. *J. Am. Chem. Soc.* **1970**, *92*, 4786.
(37) Radom, L.; Hehre, W. J.; Pople, J. A. *J. Am. Chem. Soc.* **1972**, *94*, 2371.
(38) Douglas, D.; Schleyer, P. v. R. *J. Org. Chem.* **1990**, *55*, 1003.
(39) Millefiori, S.; Alparone, A. *J. Chem. Soc., Faraday Trans.* **1998**, *94*, 25.
(40) Reed, A. E.; Weinstock, R. B.; Weinhold, F. *J. Chem. Phys.* **1985**, *83*, 735.
(41) Bader, R. F. W. *Atoms in Molecules, A Quantum Theory*; Claredon Press: Oxford, 1990.
(42) Brain, P. T.; Morrison, C. A.; Parsons, S.; Rankin, D. W. H. *J. Chem. Soc., Dalton Trans.* **1996**, 4589. Blake, A. J.; Brain, P. T.; McNab, H.; Miller, J.; Morrison, C. A.; Parsons, S.; Rankin, D. W. H.; Robertson, H. E.; Smart, B. A. *J. Phys. Chem. A* **1996**, *100*, 12280. Mitzel, N. W.; Rankin, D. W. H. *Dalton Trans.* **2003**, 3650.
(43) Sipachev, V. A. *J. Mol. Struct.* (*THEOCHEM*) **1985**, *121*, 143.
(44) Durig, J. R.; Zhou, L.; Schwartz, T.; Gounev, T. *J. Raman Spectrosc.* **2000**, *31*, 193.
(45) Fernández, L. E.; Ben Altabef, A.; Varetti, E. L. *J. Mol. Struct.* **1998**, *444*, 227.
(46) Fernández, L. E.; Ben Altabef, A.; Varetti, E. L. *J. Mol. Struct.* **2002**, *612*, 1.
(47) Della Védova, C. O. *Spectrochim. Acta, Part A* **1991**, *47*, 1619.
(48) Fogarasi, G.; Zhou, X.; Taylor, P. W.; Pulay, P. *J. Am. Chem. Soc.* **1992**, *114*, 8191.
(49) Pulay, P.; Fogarasi, G.; Pongor, G.; Boggs, J. E.; Vargha, A. *J. Am. Chem. Soc.* **1983**, *105*, 7037.
(50) Kalincsák, F.; Pongor, G. *Spectrochim. Acta, Part A* **2002**, *58*, 999.